J Mater Sci: Mater Electron (2021) 32:10458–10472

Role of nickel doping on magnetocaloric properties of $La_{0.7}Sr_{0.3}Mn_{1-x}Ni_xO_3$ manganites

Selda Kılıç Çetin[1,*], Gönül Akça[2], Mehmet Selim Aslan[2], and Ahmet Ekicibil[2]

[1] Central Research Laboratory, Çukurova University, 01330 Adana, Turkey
[2] Department of Physics, Faculty of Sciences and Letters, Çukurova University, Adana, Turkey

Received: 26 January 2021
Accepted: 6 March 2021
Published online: 20 March 2021

ABSTRACT

This study reports the effect of Ni substitution for Mn on structural, magnetic, and magnetocaloric properties of $La_{0.7}Sr_{0.3}MnO_3$ manganite synthesized by sol–gel technique. The structural, morphological, and magnetic properties are investigated using x-ray diffractometer (XRD), scanning electron microscope (SEM), and vibrating sample magnetometer (VSM) systems. XRD results showed that all samples crystallize in rhombohedral structure. Thermomagnetic measurements showed that T_C decreases with the addition of Ni from 363 K for x = 0.00 to 324 K for x = 0.06. ΔS_M determined by Maxwell's relations and Landau theory gave compatible results in the transition temperature and region above. ΔS_M^{max} values were determined as 4.52, 4.51, 4.41, and 3.90 J kg^{-1} K^{-1} for x = 0.00, 0.02, 0.04, and 0.06 at 5T, respectively. The Arrott plots and the scaling analysis of ΔS_M, which collapsed on a single curve, showed that magnetic transitions are of second order.

1 Introduction

Because of global warming and climate change, our dependence on air conditioning and cooling systems is increasing day by day to improve our living standards. This situation causes an enhancement of energy consumption in these areas. Energy consumption must be kept under control for the development of countries in all areas. Therefore, countries have to make regulations and they study to improve new systems with low energy consumption. Among the existing and studied cooling and air conditioning systems, magnetic refrigeration (MR) systems have been quite hopeful because of high energy efficiency and low energy consumption [1] when compared to conventional gas compression systems extensively using in all areas. These systems have quite good properties environmentally [2]. In addition, these systems also have low cost and noise [3]. MR systems work according to magnetocaloric effect (MCE). Briefly, this effect is defined as the temperature change of a magnetic material under magnetic field [2]. Except refrigeration, the MCE has drawn interest for the conversion and harvesting of the energy [4] and medical area (such as drug delivery and hyperthermia) [5].

Address correspondence to E-mail: kilics@cu.edu.tr

https://doi.org/10.1007/s10854-021-05702-2

Magnetic entropy change (ΔS_M) and adiabatic temperature (T_{ad}) change are two magnitudes which are defining the MCE [6]. All magnetic materials show magnetocaloric (MC) properties because of it being an internal property of the materials [7]. The basic purpose of the studies on the MCE is to provide the appropriate cooling element for MR systems [5, 8, 9]. The MC materials have to meet certain requirements in order to be used in MR applications [2, 3]. Since the discovery of the MCE,different families of materials that may be suitable for MR systems have been identified [8–14]. Among these material families, $RE_{1-x}A_xMnO_3$ perovskite manganites (where RE states rare earth elements and A points out monovalent or divalent elements) have been investigated intensively for their physical properties [15–20]. The physical properties of manganite materials are affected by several factors such as sample production method, chemical stoichiometry, and the type of metal ion [21]. The type of metal ion replaced by the A- or Mn-site changes the double-exchange (DE) interaction. Consequently, this affects the magnetic and MC properties of the samples. There are some studies showing the effect of element replacing such as Co, Cr, Cu, and Ni by Mn on magnetic and MC properties [21–25]. In these studies, it is aimed to obtain materials that can be used as candidate refrigerant material for MR systems.

One of the perovskite manganite family, La-based $La_{0.7}Sr_{0.3}MnO_3$ compound has been attracted quite due to its high magnetic phase transition temperature and high colossal magnetoresistive value [26]. To improve the physical properties and attain deep information of $La_{0.7}Sr_{0.3}MnO_3$ compound, the $La_{0.7}Sr_{0.3}MnO_3$ compound has been prepared by using different techniques [26–28]. Furthermore, by making dopings/substitutions to both of A- and B-site, the effects on physical properties have been investigated [23, 24, 26, 27, 29–31]. This study reports the effect of Ni-doped $La_{0.7}Sr_{0.3}Mn_{1-x}Ni_xO_3$ ($0 \le x \le 0.06$) manganites prepared by sol–gel technique on the structural, magnetic, and MC properties.

2 Experimental procedure

$La_{0.7}Sr_{0.3}Mn_{1-x}Ni_xO_3$ ($0.00 \le x \le 0.06$) manganite samples abbreviated as LSM, LSM2, LSM4, and LSM6, respectively, have been produced by sol–gel technique. To synthesize the sample, $La(NO_3)_3{\cdot}6H_2O$, SrO, NiO and $Mn(NO_3)_2{\cdot}6H_2O$ compounds are used. The processes of the sol–gel method are given in the previous studies [32]. To obtain the samples targeted, stoichiometric ratios of the initial materials firstly were solved in optimum solvents. The solutions were mixed by the magnetic stirrer at a certain temperature. To obtain gel form, auxiliary chemicals were added to the solutions in appropriate proportions. To obtain the dried form, the samples were heated on a hot plate. The final samples were calcined 600 °C for 6 h. The sintering temperature and time for the sample is 1200 °C and 24 h, respectively. The structural properties and grain structure of the samples were investigated by using x-ray diffractometer (XRD) with a PANalytical-EMPYREAN diffractometer and scanning electron microscope (SEM) using a FEI-Quanta 650 Field Emission microscope. To identify the magnetic properties and compute the value of ΔS_M for the samples, magnetization measurements vs. temperature ($M(T)$) and magnetic field ($M(H)$) were performed by using physical properties measurement systems (PPMS) with a vibrating sample magnetometer (VSM) option of Quantum Design PPMS DynaCool-9. The $M(T)$ measurements were performed at the temperature interval between 5–380 K under a magnetic field of 10 mT. After determining the magnetic phase transition temperature of the samples, the $M(H)$ measurements were made with 4 K temperature increments in the transition temperature range up to 5T.

3 Results and discussions

Figures 1a–d show the XRD spectra taken at room temperature for $La_{0.7}Sr_{0.3}Mn_{1-x}Ni_xO_3$ ($0.00 \le x \le 0.06$) manganites. As seen from the figure, the diffraction patterns of all samples are similar to each other, and it is observed that there is no detectable secondary phase. The diffraction peaks were indexed in the rhombohedral structure. Lattice parameters and unit cell volume of the samples are specified by using Fullprof software and these values are given in Table 1. As seen from Table 1, the unit cell volume of the samples decreases with increasing Ni concentration. This decreasing may be explained by Ni^{2+} ionic radius (0.55 Å) which is smaller than Mn^{3+} (0.65 Å). Even though the unit cell volume and lattice parameters change with Ni^{2+} content, no change in crystal structure was observed. These

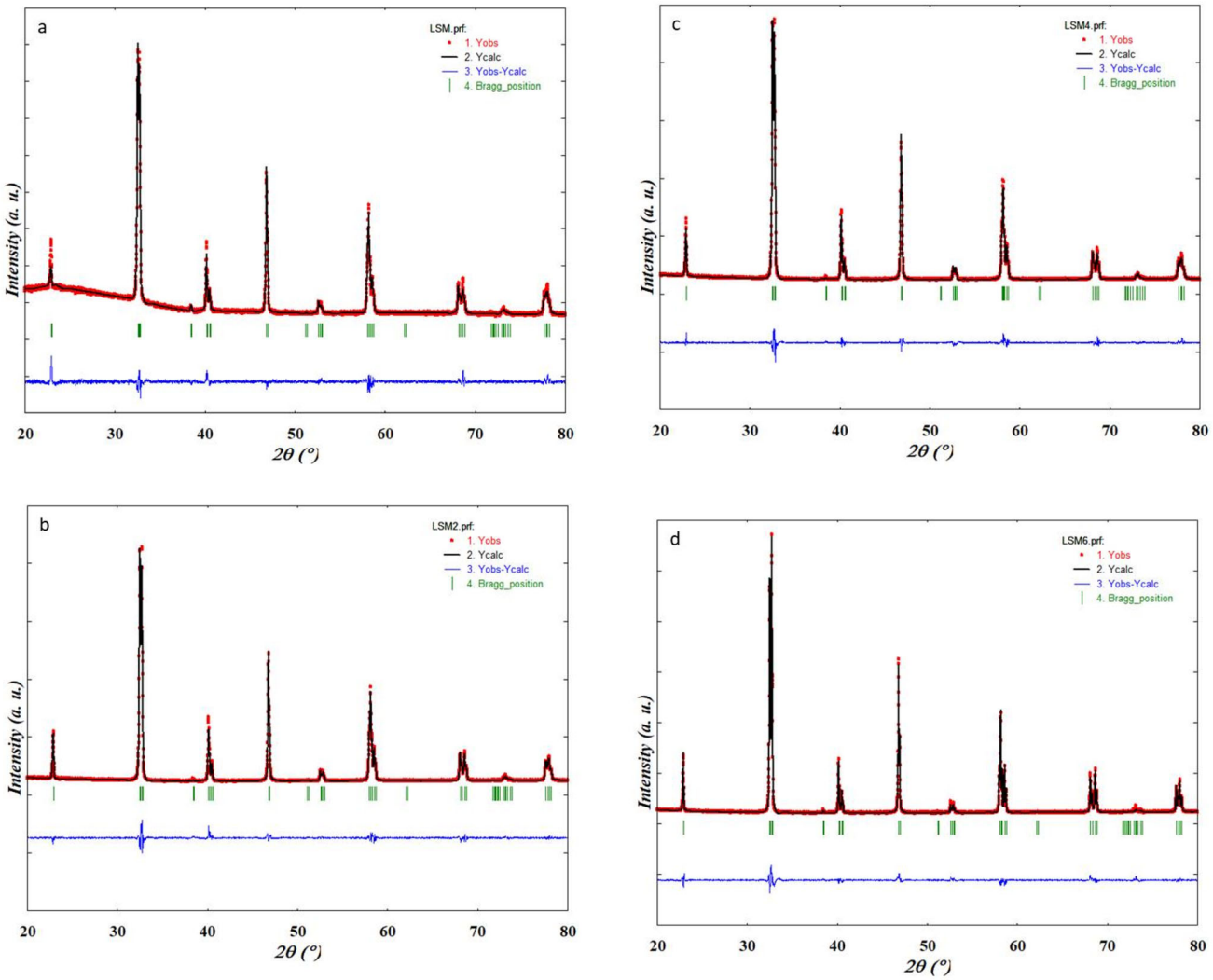

Fig. 1 The XRD pattern of $La_{0.7}Sr_{0.3}Mn_{1-x}Ni_xO_3$ ($x = 0.00$, 0.02, 0.04, 0.06) samples. The observed and calculated data are solid circle (red) and solid line (black), respectively. The blue line is the difference between the observed and calculated data. The positions of Bragg position reflection are represented by vertical green ticks

Table 1 The lattice parameters, unit cell volume, A-site, and Mn-site radius, tolerance factor t, and grain sizes of $La_{0.7}Sr_{0.3}Mn_{1-x}Ni_xO_3$ samples

x	a (Å)	b (Å)	c (Å)	V (Å^3)	$\langle r_A \rangle$ (Å)	$\langle r_{Mn} \rangle$ (Å)	t	Grain size (μm)
0.00	5.5006	5.5006	13.3531	349.8966	1.384	0.6105	0.9792	0.361
0.02	5.5045	5.5045	13.3563	350.4693	1.384	0.6095	0.9798	0.492
0.04	5.5014	5.5014	13.3501	349.9143	1.384	0.6084	0.9802	0.414
0.06	5.5015	5.5015	13.3395	349.6491	1.384	0.6063	0.9812	0.407

changes in the structural properties of the samples are expected to cause variation in the magnetic and MC properties of the compounds. The structural results obtained in this study are similar to the literature [33, 34].

Manganites are found in perovskite structure and it is controlled by equation formulized with $t = (r_A + r_O)/\sqrt{2}(r_{Mn} + r_O)$ which is known as tolerance factor (t). It is a dimensional criterion that depends on the sizes of the ions and characterizes the distinct structures derived from the perovskite structures. In the equation, the ionic radii of the A cation, B cation, and oxygen are represented by r_A, r_B, and r_O, respectively. The values of r_A and r_B are given in Table 1. In ideal

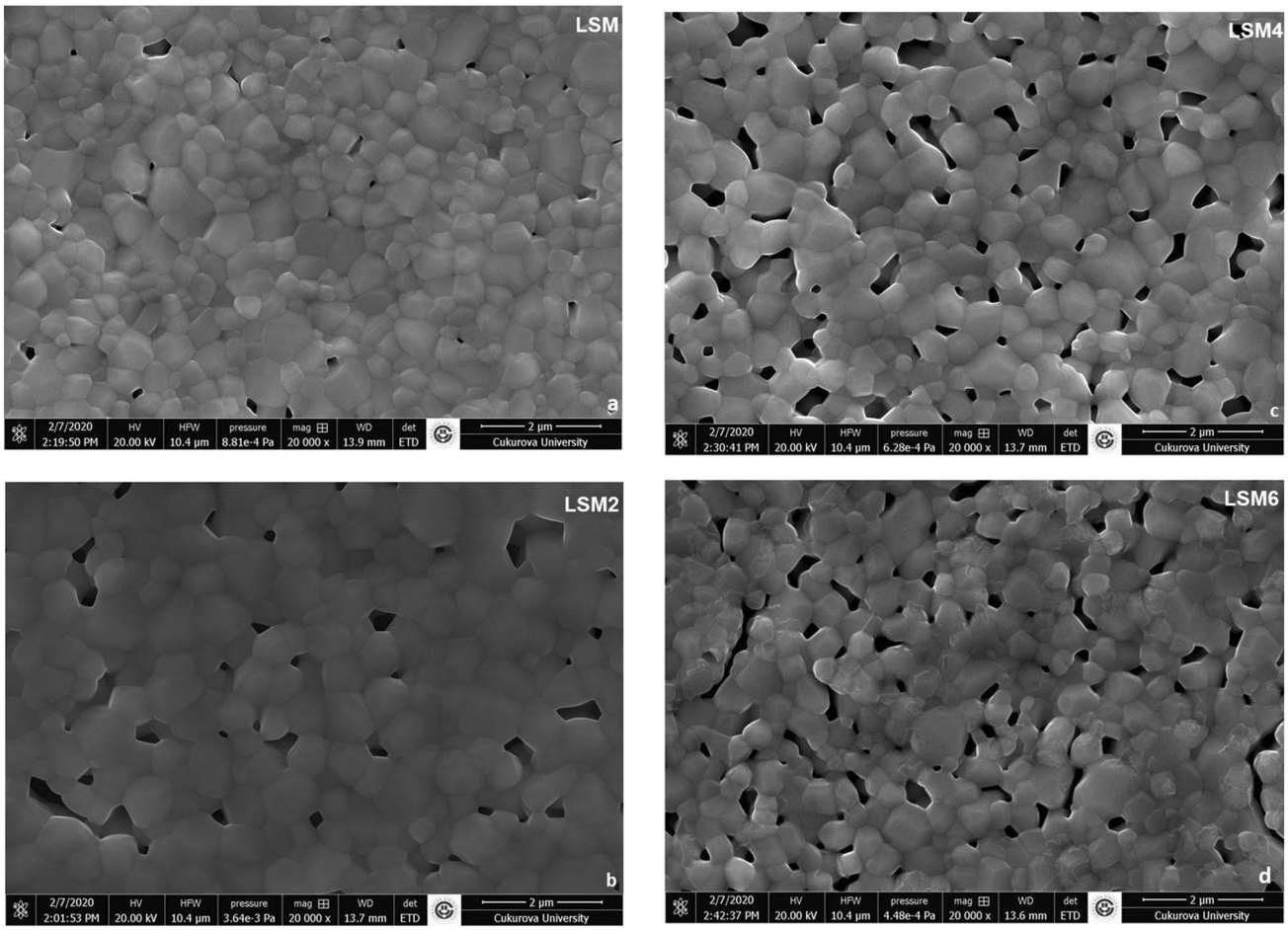

Fig. 2 SEM images of $La_{0.7}Sr_{0.3}Mn_{1-x}Ni_xO_3$ (x = 0.00, 0.02, 0.04, 0.06) samples taken at 20 KX magnifications

perovskites, t is equal to one and crystal structure is cubic. But, the crystal structure of the materials covaries with the change of the t value. [35]. For rhombohedral structure, t values are between 0.96 and 1.0 [36]. By using Shannon's Table [37], we have calculated the average radii of A- and B-sites as well as t value and these values are given in Table 1. The t value for the samples increases with increasing Ni ratio in the system from 0.9792 for x = 0.00 to 0.9812 for x = 0.06. When Ni is added instead of Mn, according to the neutrality equation ($La^{3+}_{0.7}Sr^{2+}_{0.3}Mn^{3+}_{0.7-x}Mn^{4+}_{0.3+x}Ni^{2+}_{x}O^{2-}_{3}$) [38], Mn^{3+} decreases while Mn^{4+} increases. In case, if a decrease in the average ionic size of the B-site occurs, the average ionic size of B-site decreases and the t values increase. The calculated t values affirm that the crystal structure of the samples is rhombohedral.

Morphological properties of the samples affect the magnetic and MC properties of the samples. Therefore, the morphology of the samples was investigated using SEM at 20 KX magnifications. The SEM images of the samples are given in Fig. 2. From SEM images, it is seen that grains have slightly different sizes and polygonal volume particle structures, mostly spherical, and the grain boundary is clear for all samples. The grain sizes of the samples are calculated by using Image J software and are seen in Table 1. The histograms of the grain size are given in Fig. 3. It is observed that the grain size is reduced with increasing Ni concentration.

The elemental analyzes of the samples were performed using SEM with equipment energy dispersive x-ray spectroscopy (EDS). Figure 4 shows the EDS spectra of the samples. All elements seen from EDS peak reflections belong to the elements that form the samples. The peak reflection of any element other than the compounds used in the sample production process was not scanned. In addition, it can be seen from the EDS spectra that the number and intensity of Ni peaks increase in proportion to the increase in

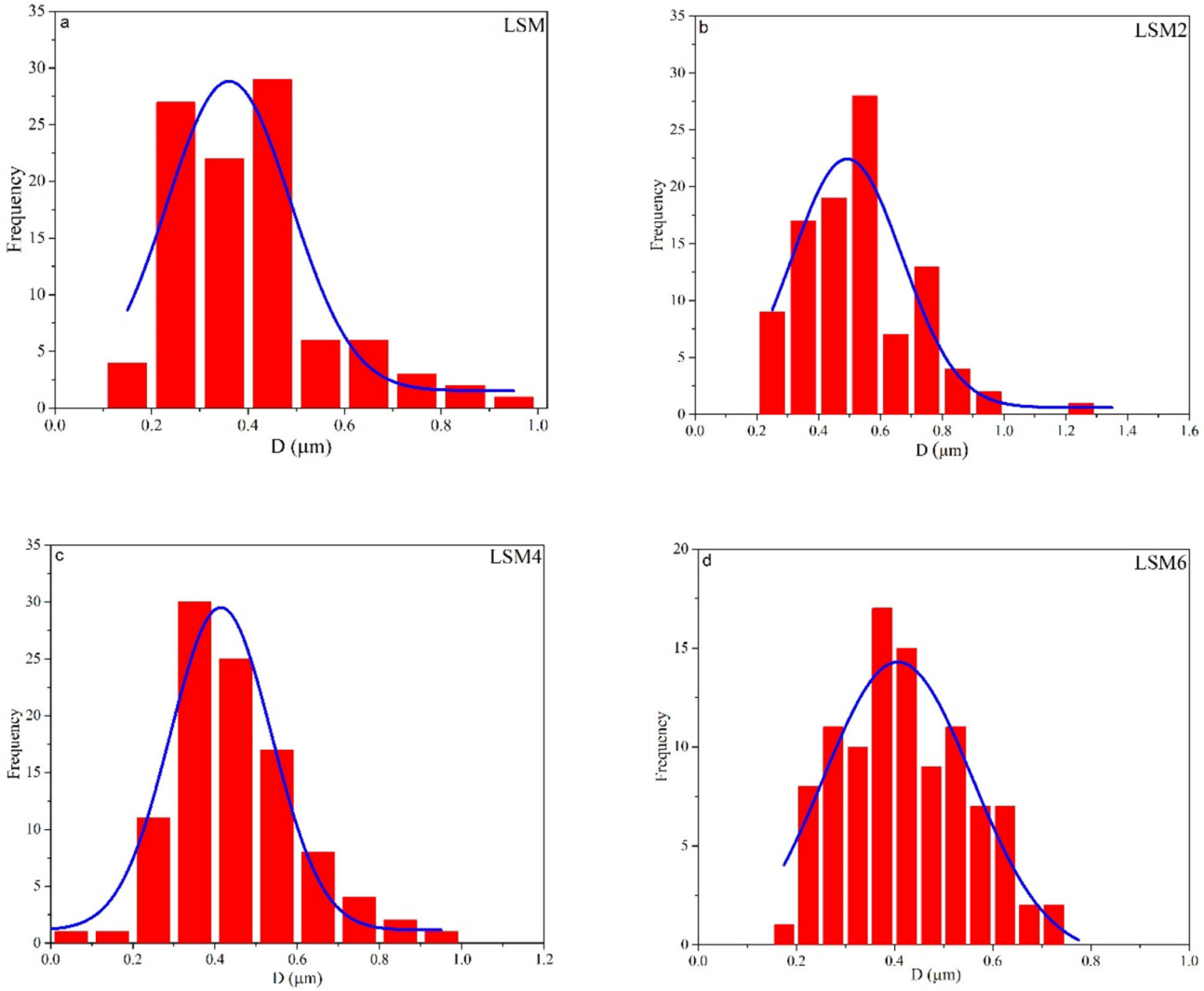

Fig. 3 The size distribution histogram of $La_{0.7}Sr_{0.3}Mn_{1-x}Ni_xO_3$ (x = 0.00, 0.02, 0.04, 0.06) samples

Ni concentration. Atomic percentages of the elements that compose the compound according to the results of the EDS analysis are given in Table 2. According to the chart, it is seen that the elements forming the compounds do not suffer any loss during production.

Thermomagnetic measurements were carried out to study the magnetic behavior of $La_{0.7}Sr_{0.3}Mn_{1-x}Ni_xO_3$ ($0.00 \leq x \leq 0.06$) samples and to determine their transition temperatures. Figure 5 shows the zero-field cooling (ZFC) and field cooling (FC) magnetization curves in the temperature range 5–380 K under 10 mT. From the magnetization curves, it is seen that the samples change from the ferromagnetic (FM) to the paramagnetic (PM) with increasing the temperature. As thermal interaction energy increases with the increase of temperature, the FM coupling is disrupted and consequently magnetization rapidly decreases to zero at a temperature. This temperature is called as Curie temperature (T_C). As seen in figure, while the ZFC and FC curves overlap in the PM region, it is seen that the curves diverge when moving towards the FM region. Since the highest separation is observed in the LSM4 sample, we can say that the most anisotropy is in this sample. Another situation that confirms the high anisotropy of this material is that the magnetization increases as the temperature decreases in the FC curve. In cases where anisotropy is low, the magnetization value follows a constant path with temperature decrease. The T_C values of the samples were determined as 363, 351, 344, and 324 K for LSM, LSM2, LSM4, and LSM6, respectively. From the results, it is seen that T_C

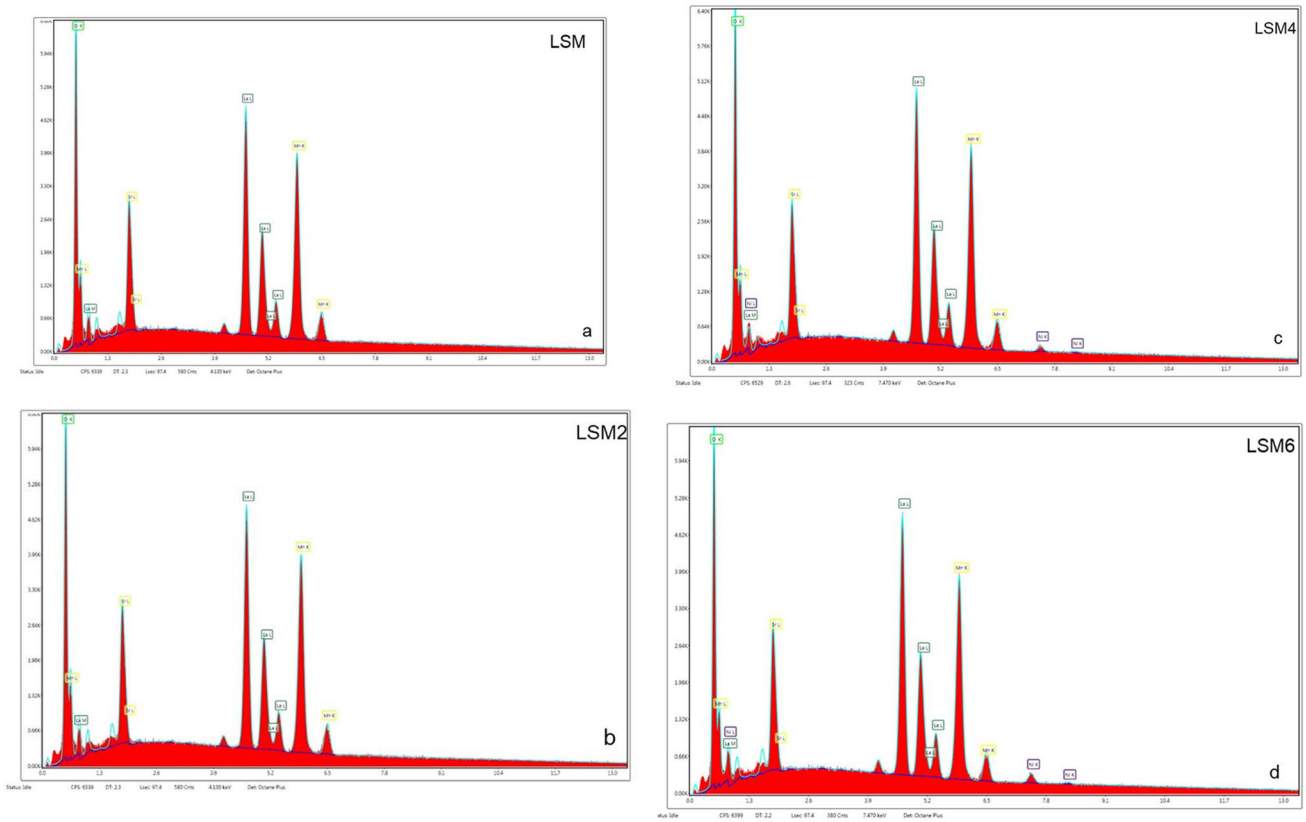

Fig. 4 EDS spectra of $La_{0.7}Sr_{0.3}Mn_{1-x}Ni_xO_3$ (x = 0.00, 0.02, 0.04, 0.06) samples

Table 2 The atomic percentage of the $La_{0.7}Sr_{0.3}Mn_{1-x}Ni_xO_3$ samples

x	Atomic percentage				
	La	Sr	Mn	Ni	O
0.00	14.37	5.48	20.26	0	59.89
0.02	14.72	5.41	20.76	0.48	58.63
0.04	14.75	5.28	20.14	0.82	59.00
0.06	14.62	5.51	19.70	1.33	58.84

decreases as the amount of Ni replaced by Mn increases. Ni doping in the Mn region causes an increase in the number of ions from the Mn^{3+} state to the Mn^{4+} state. The transformation of the $Mn^{3+}\left(t_{2g}^3, e_g^1\right)$ ion to the $Mn^{4+}\left(t_{2g}^3, e_g^0\right)$ state is defined as the hole (space) doping [39]. The Mn^{4+}/Mn^{3+} ratio formed with the addition of Ni to the structure was calculated as 0.43, 0.48, 0.55, and 0.62 for LSM, LSM2, LSM4, and LSM6, respectively. Thus, it can be said that with the increase of Ni amount, a decrease in the T_C is observed due to the decrease in the number of conduction electrons. In addition, newly formed Mn^{3+}–O–Ni^{2+}, Mn^{4+}–O–Mn^{4+}, and Ni^{2+}–O–Ni^{2+} bond interactions will weaken the FM double-exchange interactions and support the antiferromagnetism with the substitution of Mn by Ni^{2+} ions [34]. As a result, the T_C gradually decreases as the amount of Ni increases.

After the determination of the T_C temperatures, isothermal magnetization measurements were taken in this temperature region in order to determine the ΔS_M, which are mostly changing in this region. The $M(H)$ measurements were carried out in the T_C region in 4 K temperature steps up to 5T applied magnetic field and are shown in Fig. 6 for the samples. As can be seen clearly from Fig. 6, $M(H)$ curves lead to the saturation particular to FM state at low temperatures, while they are in the form of linear curves specific to PM state at temperatures above the T_C.

To determine the magnitude of the MCE, the ΔS_M values of the samples from the isothermal magnetization curves are calculated using the approximated Maxwell's thermodynamic relation [40]:

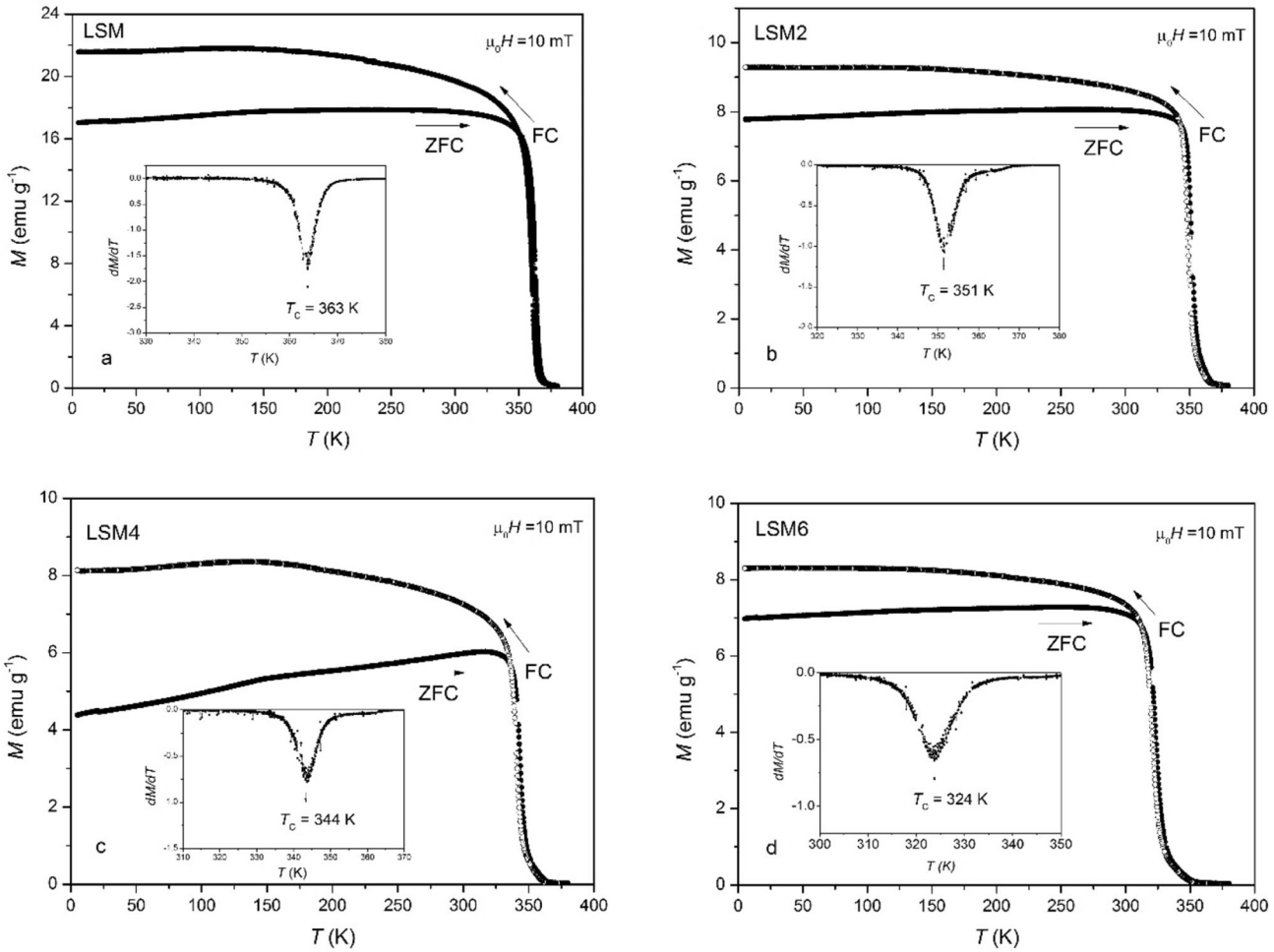

Fig. 5 $M(T)$ curves of $La_{0.7}Sr_{0.3}Mn_{1-x}Ni_xO_3$ (x = 0.00, 0.02, 0.04, 0.06) samples. Insets: temperature dependence of dM/dT

$$|\Delta S_M| = \sum_i \frac{M_i - M_{i+1}}{T_{i+1} - T_i} \Delta H, \quad (1)$$

where M_i and M_{i+1} are the magnetizations at T_i and T_{i+1}, respectively. The temperature-dependent ΔS_M curves obtained at different magnetic fields are given in Fig. 7. Since the ΔS_M is a magnitude proportional to change of magnetization, it goes to a maximum in the T_C region where the greatest change occurs. From Fig. 7, it is seen that the ΔS_M curves of the samples go to maximum at their T_C temperatures, supporting this explanation. With the increase in the applied magnetic field value, the ΔS_M values increased, as expected, depending on the increase in the number of magnetic moments in the direction of the magnetic field. Furthermore, the peak of ΔS_M curves over a wide temperature range reveals that the magnetic phase transition has a second-order character [41]. The maximum magnetic entropy change (ΔS_M^{max}) values are determined as in Table 3 at different magnetic fields. These values are larger than the results given in the literature of doping to Mn-site in different manganite materials [34, 42–45]. It is clear from Table 3 that the ΔS_M^{max} values decreased with the increase of Ni amount as in the T_C. This decrement is due to the decrease in the number of conduction electrons, which also causes a decrease in the T_C due to the increase in the number of $Mn^{4+}\left(t_{2g}^3 e_g^0\right)$ ions with addition of Ni to the structure.

Relative cooling power (RCP) expresses technological importance of the MCE and refers to the amount of heat transferred from the hot to cold sinks in an ideal refrigerant cycle [46]. The RCP value of a material can be evaluated from the equation below:

$$RCP = -\Delta S_M^{max} \times \delta T_{FWHM} \quad (2)$$

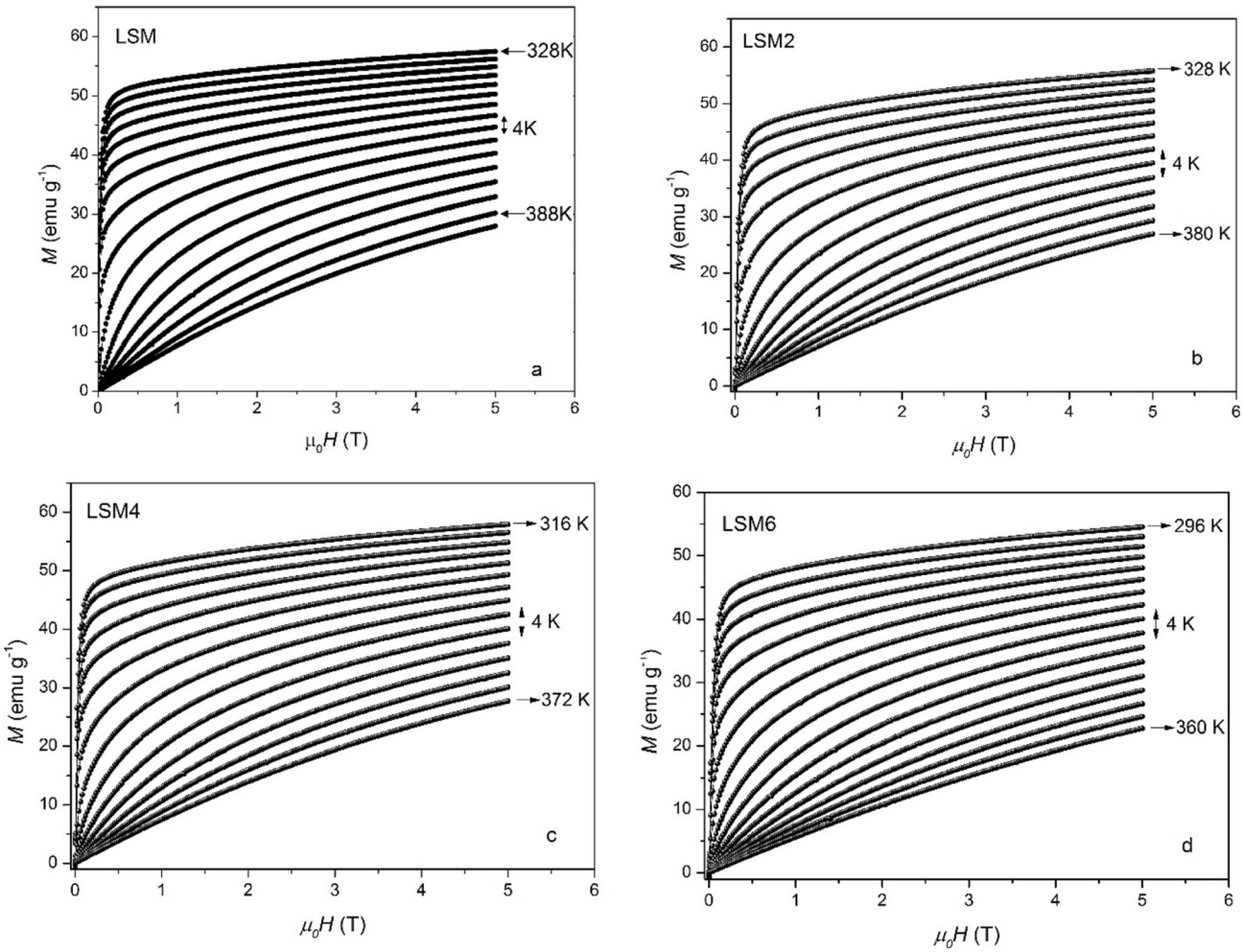

Fig. 6 $M(H)$ curves of $La_{0.7}Sr_{0.3}Mn_{1-x}Ni_xO_3$ (x = 0.00, 0.02, 0.04, 0.06) samples

where δT_{FWHM} shows full width of the ΔS_M curve at half maximum [46]. RCP values are calculated for all samples and shown in Table 3. Initially, the RCP value increased with the expansion of the temperature range of the ΔS_M curve with the addition of Ni to the structure, but it systematically decreased with the increase of the Ni concentration.

For the purpose of understanding the nature of the transition from FM to PM state, curves of H/M vs. M^2, called as Arrott plots, are evaluated from these $M(H)$ curves. Figure 8 shows the Arrott plots for all samples. The Banerjee criterion [47] states that the magnetic phase transition has a second-order transition if the Arrott curves around the T_C have a positive slope and a first-order transition otherwise. From Fig. 8, it can be said that the samples have a second-order transition due to their positive slope in T_C region. Materials showing second-order magnetic phase transition are more advantageous than those with first-order transition because they have low thermal and magnetic hysteresis, which is of great importance for technological requirements [48]. It is seen from the Arrott curves of each sample at its transition temperature that the curves pass through the origin. This signifies that there is a true long range FM interaction [42]. Another method that verifies the second-order phase transition is the universal master curve proposed by Franco [49]. In this method, ΔS_M values are normalized to its maximum value and the temperature axis is rescaled according to the equations below [49].

$$\theta = \begin{cases} -(T - T_C)/(T_{r1} - T_C)T \leq T_C \\ (T - T_C)/(T_{r2} - T_C)T > T_C \end{cases} \quad (3)$$

where T_{r1} and T_{r2} are the temperatures below and above T_{peak}. These temperatures are values corresponding to the arbitrary value of $h < 1$ to ΔS_M

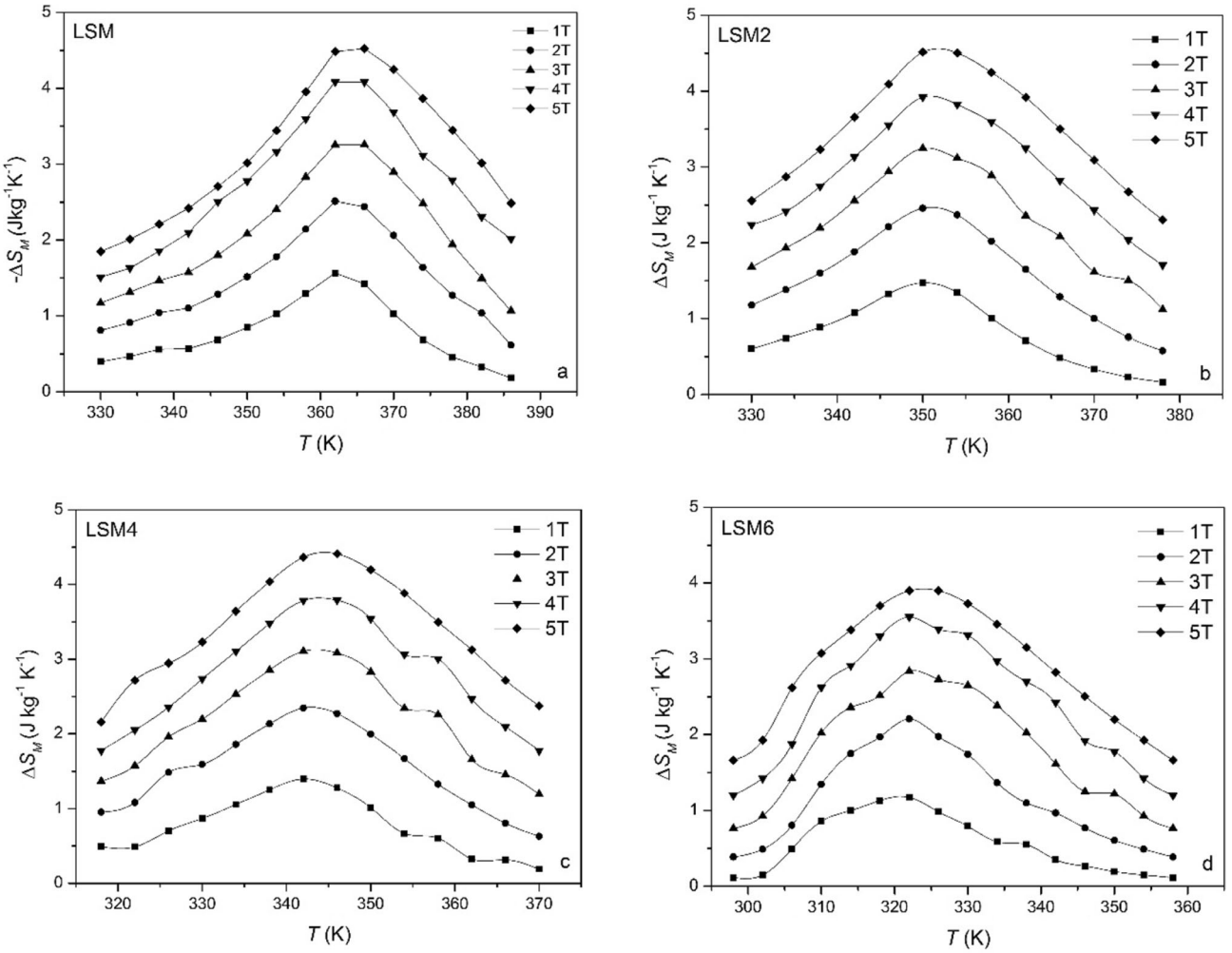

Fig. 7 $\Delta S_{\mathrm{M}}(T)$ curves of $La_{0.7}Sr_{0.3}Mn_{1-x}Ni_xO_3$ (x = 0.00, 0.02, 0.04, 0.06) samples at different applied magnetic fields

Table 3 Curie temperature, T_{C}, relative cooling power, RCP, and maximum magnetic entropy change $-\Delta S_M^{\max}$ for $La_{0.7}Sr_{0.3}Mn_{1-x}Ni_xO_3$ samples

x	T_{C} (K)	RCP (J kg^{-1}) (5T)	$-\Delta S_M^{\max}$ (J kg^{-1} K^{-1})				
			1 T	2 T	3 T	4 T	5 T
0.00	363	219	1.57	2.51	3.26	4.09	4.52
0.02	351	235	1.47	2.46	3.25	3.92	4.51
0.04	344	233	1.40	2.35	3.11	3.79	4.41
0.06	324	200	1.17	2.21	2.84	3.55	3.90

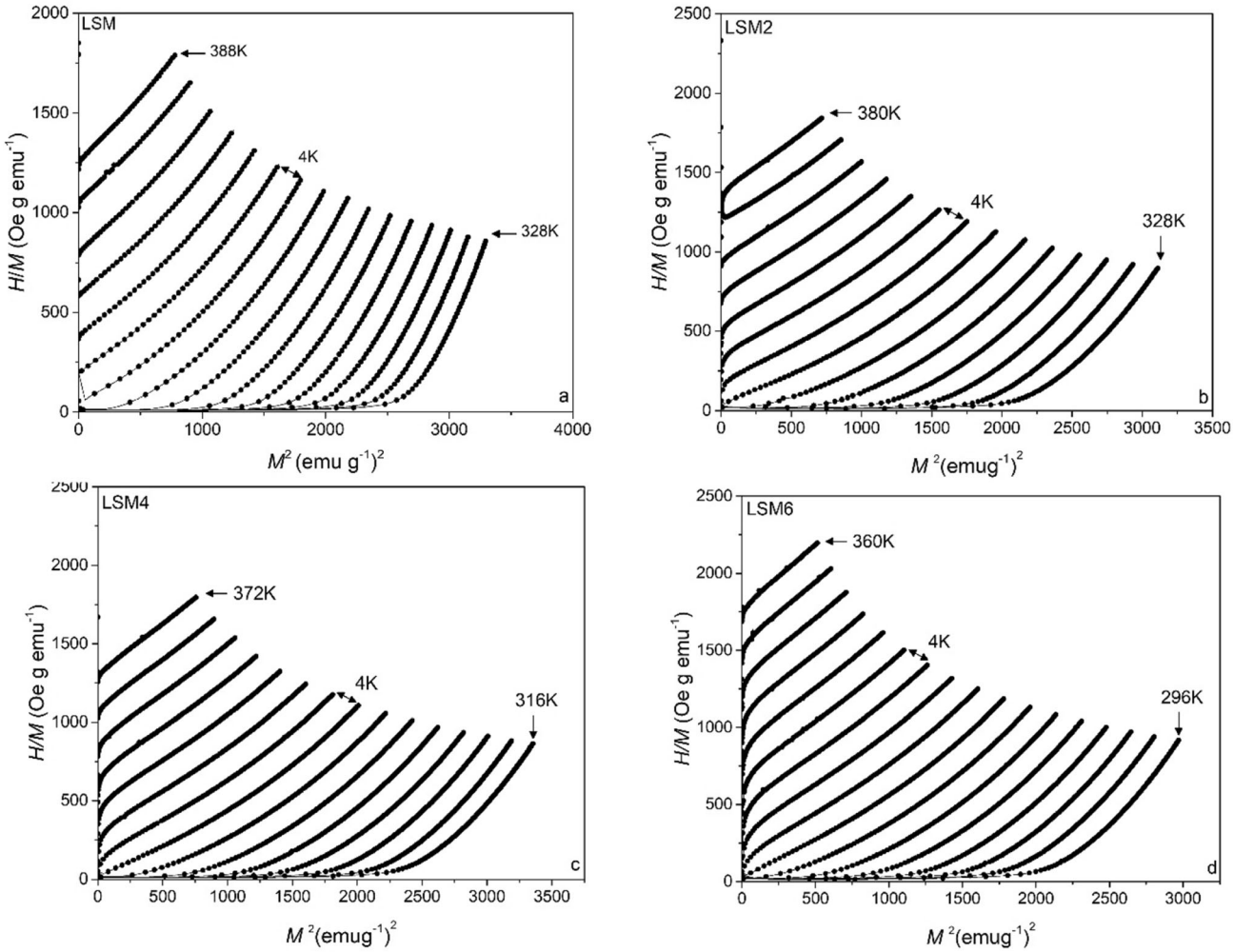

Fig. 8 Arrott plots of $La_{0.7}Sr_{0.3}Mn_{1-x}Ni_xO_3$ (x = 0.00, 0.02, 0.04, 0.06) samples

$(T_{r1,2})/\Delta S_M^{peak} = h$. Figure 9 shows the normalized ΔS_M vs. θ at different applied fields. It is clear from the figure that the normalized entropy change curves overlap on a single curve for all samples. This shows that the magnetic phase transition is second order.

To identify the magnetic phase transition's order, the Landau theory which takes into account the electron interaction and magnetoelastic coupling effects is also used [50]. For a sample exhibiting second-order phase transition at temperatures near T_C, the Gibbs free energy depended on magnetization and temperature can be written as the following equation:

$$G(M,T) = \frac{a(T)}{2}M^2 + \frac{b(T)}{4}M^4 + \frac{c(T)}{6}M^6 + \cdots - \mu_0 H. \quad (4)$$

In Eq. (4), the terms of *a*, *b*, *and c* are known as Landau coefficients. The temperature dependence of Landau coefficients has been calculated for all samples, and the ones for LSM and LSM6 manganite are given in Fig. 10a–b. Information about the type of the magnetic phase transition can be provided from the Landau theory. [19, 51]. The *a* coefficient gets a minimum value at temperatures near T_C. The *b* coefficient including the elastic and the magnetoelastic terms of free energy determines the type of magnetic phase transition [52]. If the *b* coefficient is positive at T_C, it is second order [53]. Around T_C, the value of the *b* coefficient is positive for the samples as seen from Fig. 10a–b. This expresses that the phase transition for the samples is of second order. The *c* coefficient affected by experimental errors is a constant. This coefficient is always positive at T_C [54].

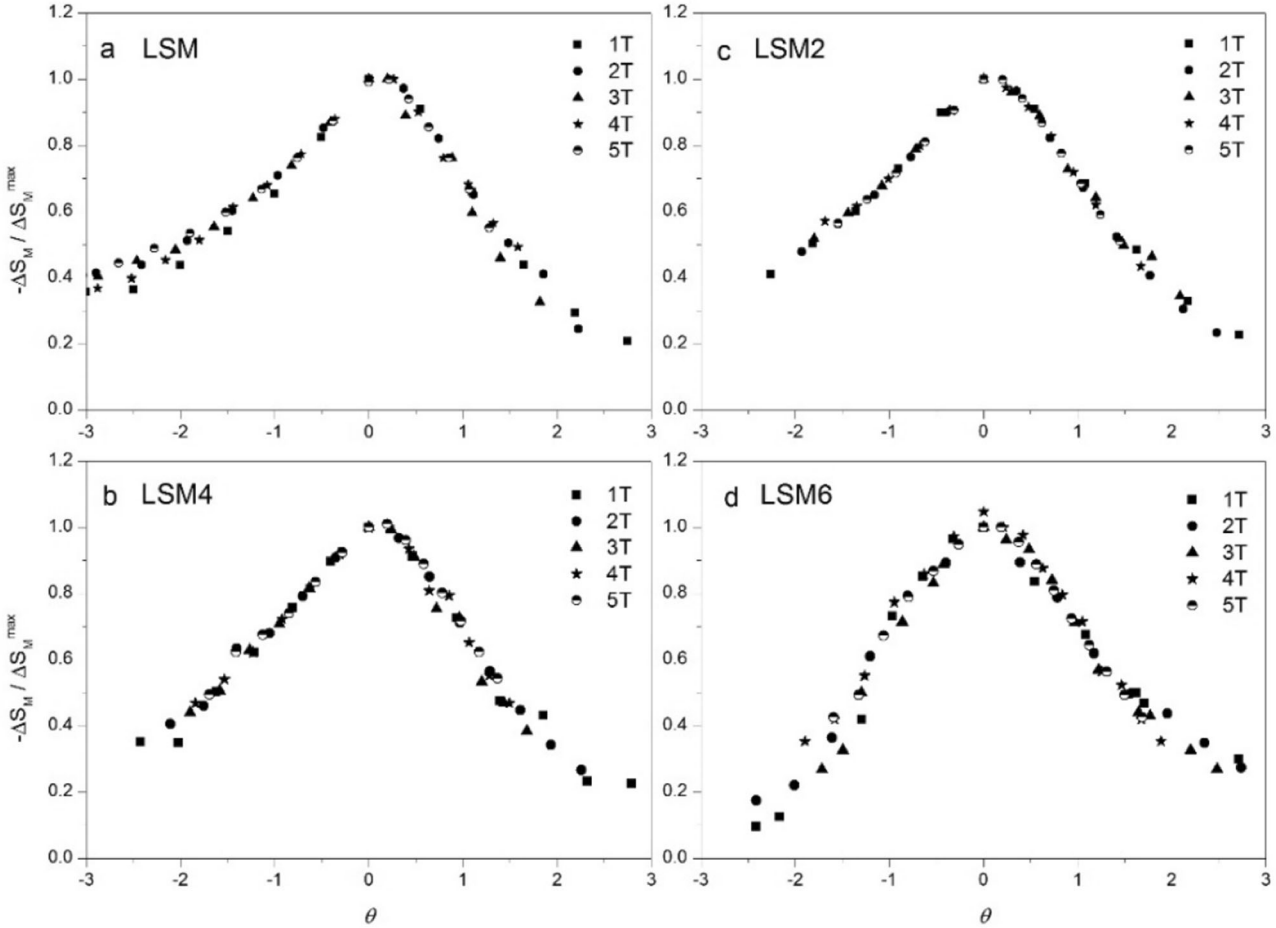

Fig. 9 Rescaled temperature θ versus normalized magnetic entropy change curves at different magnetic field for $La_{0.7}Sr_{0.3}Mn_{1-x}Ni_xO_3$ (x = 0.00, 0.02, 0.04, 0.06) samples

According to the energy minimization, for a magnetic system, the equation of state system can be given as follows:

$$\frac{H}{M} = a(T) + b(T)M^2 + c(T)M^4 \tag{5}$$

The theoretical $-\Delta S_M$ value of the FM materials is computed by

$$-\Delta S_M = \left(\frac{\partial G}{\partial T}\right)_H = \frac{1}{2}a'(T)M^2 + \frac{1}{4}b'(T)M^4 + \frac{1}{6}c'(T)M^6 \tag{6}$$

Figure 10c shows the temperature dependence of the theoretical and experimental $-\Delta S_M$ curves for 5T. The obtained $-\Delta S_M$ are in agreement with each other above T_C temperatures. This result gives information that the magnetoelastic coupling and electron interactions may alter both $-\Delta S_M$ values and the temperature dependence of the $-\Delta S_M$ curves [55, 56]. Below T_C temperatures, there are differences between the obtained experimental values. This may arise from the Jahn–Teller effect, exchange interactions, and micromagnetism [57].

4 Conclusions

The effect of Ni substitution with Mn in $La_{0.7}Sr_{0.3}MnO_3$ manganite on structural, magnetic, and MC properties was studied. Sol–gel technique was used in synthesis samples. It has been observed from XRD spectra that the samples have mono-phase and rhombohedral symmetry. $M(T)$ showed that the samples change from the FM to the PM state with increasing the temperature. T_C temperatures are determined as 363, 351, 344, and 324 K for LSM, LSM2, LSM4, and LSM6, respectively. The T_C decreased with the increase of the Ni concentration.

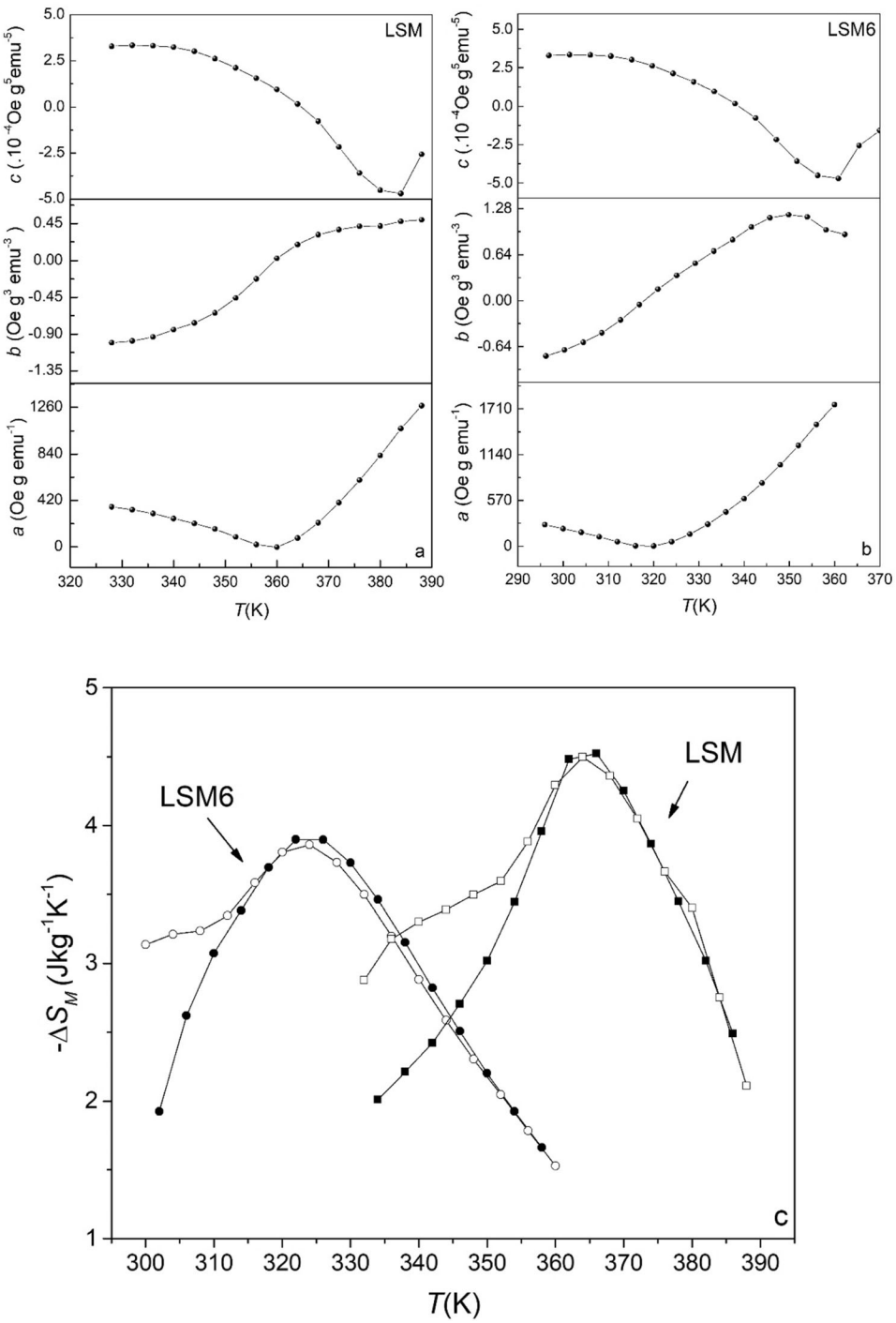

Fig. 10 The temperature dependence of the Landau coefficients for **a** LSM and **b** LSM6. The temperature dependence of the experimental and theoretical $-\Delta S_M$ curves for LSM and LSM6 samples under magnetic field of 5 T

This situation is attributed to the fact that the DE interaction is weakened due to the increase in the Mn^{4+} number in the structure with the increase of Ni concentration. ΔS_M of the samples was determined from the $M(H)$ measurements taken in the regions of T_C. ΔS_M^{max} values were calculated as 4.52, 4.51, 4.41, and 3.90 J kg^{-1} K^{-1} for LSM, LSM2, LSM4, and LSM6 at 5T, respectively. The magnetic phase transitions were determined as second-order from the Arrott curves and universal master curves for the samples. Results showed that the technologically important RCP values increased with the expansion of the temperature range of the ΔS_M curve with the addition of Ni to the structure. These results are important in terms of bringing the T_C of the $La_{0.7}Sr_{0.3}MnO_3$ manganite to room temperature without causing too

much decrease in ΔS_M values and with the improvement in RCP values.

Acknowledgements

This work is supported by the TUBITAK (The Scientific and Technological Research Council of Turkey) under Grant Contract No. 119F069.

References

1. B. Dorin, J. Avsec, A. Plesca, The efficiency of magnetic refrigeration and a comparison with compressor refrigeration systems. J. Energy Technol. **11**(2018), 59–69 (2018)
2. M.H. Phan, S.C. Yu, Review of the magnetocaloric effect in manganite materials. J. Magn. Magn. Mater. **308**, 325–340 (2007)
3. T. Gottschall, K.P. Skokov, M. Fries, A. Taubel, I. Radulov, F. Scheibel, D. Benke, S. Riegg, O. Gutfleisch, Making a cool choice: the materials library of magnetic refrigeration. Adv. Energy Mater. **9**, 1901322 (2019)
4. A. Kitanovski, Energy applications of magnetocaloric materials. Adv. Energy Mater. **10**, 1903741 (2020)
5. A.M. Tishin, Y.I. Spichkin, V.I. Zverev, P.W. Egolf, A review and new perspectives for the magnetocaloric effect: new materials and local heating and cooling inside the human body. Int. J. Refrig **68**, 177–186 (2016)
6. A.M. Tishin, Y.I. Spichkin, *The Magnetocaloric Effect and Its Applications* (IOP Publishing LTD, Philadelphia, 2003)
7. M. Khlifi, M. Bejar, O. EL Sadek, E. Dhahri, M.A. Ahmed, E.K. Hlil, Structural, magnetic and magnetocaloric properties of the lanthanum deficient in $La_{0.8}Ca_{0.2-x}MnO_3$ (x = 0–0.20) manganites oxides. J. Alloys Compd. **509**, 7410–7415 (2011)
8. K.A. Gschneidner, V.K. Pecharsky, A.O. Tsokol, Recent developments in magnetocaloric materials. Rep. Prog. Phys. **68**, 1479–1539 (2005)
9. C.R.H. Bahl, D. Velazquez, K.K. Nielsen, K. Engelbrecht, K.B. Andersen, R. Bulatova, N. Pryds, High performance magnetocaloric perovskites for magnetic refrigeration. Appl. Phys. Lett. **100**, (2012)
10. A.M.J. Mahdy, Overview for published magnetocaloric materials used in magnetic refrigeration applications. Int. J. Comput. Appl. Sci. IJOCAAS 3(1) (2017) ISSN: 2399-4509
11. J. Lyubina, Magnetocaloric materials for energy efficient cooling. J. Phys. D Appl. Phys. **50**, (2017)
12. O. Sari, M. Balli, From conventional to magnetic refrigerator technology. Int. J. Refrig **37**, 8–15 (2014)
13. E. Brück, O. Tegus, D.T.C. Than, N.T. Trung, K.H.J. Buschow, A review on Mn based materials for magnetic refrigeration: structure and properties. Int. J. Refrig **31**, 763–770 (2008)
14. A. Barman, S. Kar-Narayan, D. Mukherjee, Caloric effects in perovskite oxides. Adv. Mater. Interfaces **6**, 1900291 (2019)
15. N. Chau, H.N. Nhat, N.H. Luong, D.L. Minh, N.D. Tho, N.N. Chau, Structure, magnetic, magnetocaloric and magnetoresistance properties of $La_{1-x}Pb_xMnO_3$ perovskite. Phys. B **327**, 270–278 (2003)
16. M.S. Reis, V.S. Amaral, J.P. Araujo, P.B. Tavares, A.M. Gomes, I.S. Oliveira, Magnetic entropy change of $Pr_{1-x}Ca_xMnO_3$ manganites ($0.2 \leqslant x \leqslant 0.95$). Phys. Rev. B **71**, 144413–144418 (2005)
17. W. Zhong, W. Chen, C.T. Au, Y.W. Du, Dependence of the magnetocaloric effect on oxygen stoichiometry in polycrystalline $La_{2/3}Ba_{1/3}MnO_{3-\delta}$. J. Magn. Magn. Mater. **261**, 238–243 (2003)
18. G.F. Wang, L.R. Li, Z.R. Zhao, X.Q. Yu, X.F. Zhang, Structural and magnetocaloric effect of $Ln_{0.67}Sr_{0.33}MnO_3$ (Ln=La, Pr and Nd) nanoparticles. Ceram. Int. **40**, 16449–16454 (2014)
19. G. Akça, S. Kılıç Çetin, A. Ekicibil, Structural, magnetic and magnetocaloric properties of $(La_{1-x}Sm_x)_{0.85}K_{0.15}MnO_3$ (x = 0.0, 0.1, 0.2 and 0.3) perovskite manganites. Ceram. Int. **43**, 15811–15820 (2017)
20. A.O. Ayaş, M. Akyol, A. Ekicibil, Structural and magnetic properties with largereversible magnetocaloric effect in $(La_{1-x}Pr_x)_{0.85}Ag_{0.15}MnO_3$ ($0.0 \leqslant x \leqslant 0.5$) compounds. Philos. Mag. **96**, 922 (2016)
21. O. Hassayoun, M. Baazaoui, M.R. Laouyenne, F. Hosni, E.K. Hlil, M. Oumezzine, K. Farah, Magnetocaloric effect and electron paramagnetic resonance studies of the transition from ferromagnetic to paramagnetic in $La_{0.8}Na_{0.2}Mn_{1-x}Ni_xO_3$ ($0 \leq x \leq 0.06$). J. Phys. Chem. Solids **135**, (2019)
22. M.H. Phan, H.X. Peng, S.C. Yu, N.D. Tho, N. Chau, Large magnetic entropy change in Cu-doped manganites. J. Magn. Magn. Mater. **285**, 199–203 (2005)
23. N. Kallel, S. Kallel, A. Hagaza, M. Oumezzine, Magnetocaloric properties in the Cr-doped $La_{0.7}Sr_{0.3}MnO_3$ manganites. Phys. B **404**, 285–288 (2009)
24. N. Chau, P.Q. Niem, H.N. Nhat, N.H. Luong, N.D. Tho, Influence of Cu substitution for Mn on the structure, magnetic, magnetocaloric and magnetoresistance properties of $La_{0.7}Sr_{0.3}MnO_3$ perovskites. Phys. B **327**, 214–217 (2003)
25. A. Selmi, R. M'nassri, W. Cheikhrouhou-Koubaa, N.C. Boudjada, A. Cheikhrouhou, The effect of Co doping on the magnetic and magnetocaloric properties of $Pr_{0.7}Ca_{0.3}Mn_{1-x}Co_xO_3$ manganites. Ceram. Int. **41**, 7723–7728 (2015)

26. V. Dyakonov, A. Ślawska-Waniewska, N. Nedelko, E. Zubov, V. Mikhaylov, K. Piotrowski, A. Szytuła, S. Baran, W. Bazela, Z. Kravchenko, P. Aleshkevich, A. Pashchenko, K. Dyakonov, V. Varyukhin, H. Szymczak, Magnetic, resonance and transport properties of nanopowder of $La_{0.7}Sr_{0.3}MnO_3$ manganites. J. Magn. Magn. Mater. **322**, 3072–3079 (2010)
27. P.T. Phong, N.V. Dang, L.V. Bau, N.M. An, I. Lee, Landau mean-field analysis and estimation of the spontaneous magnetization from magnetic entropy change in $La_{0.7}Sr_{0.3}MnO_3$ and $La_{0.7}Sr_{0.3}Mn_{0.95}Ti_{0.05}O_3$. J. Alloys Compd. **698**, 451–459 (2017)
28. R. Cherif, S. Zouari, M. Ellouze, E.K. Hlil, F. Elhalouani, Structural, magnetic and magnetocaloric properties of $La_{0.7}Sr_{0.3}MnO_3$ manganite oxide prepared by the ball milling method. Eur. Phys. J. Plus **129**, 83 (2014)
29. R. Cherif, E.K. Hlil, M. Ellouze, F. Elhalouani, S. Obbade, Magnetic and magnetocaloric properties of $La_{0.6}Pr_{0.1}Sr_{0.3}Mn_{1-x}Fe_xO_3$ manganites. J. Solid State Chem. **215**, 271–276 (2014)
30. G. Akça, S. Kılıç Çetin, A. Ekicibil, Composite $xLa_{0.7}Ca_{0.2}Sr_{0.1}MnO_3$ /(1−x) $La_{0.7}Te_{0.3}MnO_3$ materials: magnetocaloric properties around room temperature. J. Mater. Sci.: Mater. Electron. **31**, 6796–6808 (2020)
31. H. Rahmouni, M. Nouiri, R. Jemai, N. Kallel, F. Rzigua, A. Selmi, K. Khirouni, S. Alaya, Electrical conductivity and complex impedance analysis of 20% Ti-doped $La_{0.7}Sr_{0.3}MnO_3$ perovskite. J. Magn. Magn. Mater. **316**, 23–28 (2007)
32. S. Kılıç Çetin, G. Akça, A. Ekicibil, Impact of small Er rare earth element substitution on magnetocaloric properties of $(La_{0.9}Er_{0.1})_{0.67}Pb_{0.33}MnO_3$ perovskite. J. Mol. Struct. **1196**, 658–661 (2019)
33. Y. Zhang, Local structure and magnetocaloric effect for $La_{0.7}Sr_{0.3}Mn_{1-x}Ni_xO_3$. Curr. Appl. Phys. **12**, 803–807 (2012)
34. A.E.-M.A. Mohamed, B. Hernando, A.M. Ahmed, Magnetic, magnetocaloric and thermoelectric properties of nickel doped manganites. J. Alloys Compd. **692**, 381–387 (2017)
35. R. Mouta, R.X. Silva, C.W.A. Paschoal, Tolerance factor for pyrochlores and related structures. Acta Cryst. **B69**, 439–445 (2013)
36. Z. Wang, Q. Xub, K. Chen, Maximum magnetic entropy change modulated toward room temperature in perovskite manganites La0.7−xNdx(Ca, Sr)0.3MnO3. Curr. Appl. Phys. **12**, 1153–1157 (2012)
37. R.D. Shannon, Revised effective ionic radii and systematic studies of interatomic distances in halides and chalcogenides. Acta Cryst. **A32**, 751–767 (1976)
38. K. Laajimi, M. Khlifi, E.K. Hlil, K. Taibi, M.H. Gazzah, J. Dhahri, Room temperature magnetocaloric effect and critical behavior in $La_{0.67}Ca_{0.23}Sr_{0.1}Mn_{0.98}Ni_{0.02}O_3$ oxide. J. Mater. Sci.: Mater. Electron. **13**, 11868–11877 (2019)
39. L.P. Gor'kov, V.Z. Kresin, Mixed-valence manganites: fundamentals and main properties. Phys. Rep. **400**, 149–208 (2004)
40. V.K. Pecharsky, K.A. Gschneidner Jr., Magnetocaloric effect from indirect measurements: magnetization and heat capacity. J. Appl. Phys. **86**, 565–575 (1999)
41. N. Dhahri, A. Dhahri, K. Cherif, J. Dhahr, H. Belmabrouk, E. Dhahri, Effect of Co substitution on magnetocaloric effect in $La_{0.67}Pb_{0.33}Mn_{1-x}Co_xO_3$ $(0.15\leq x\leq 0.3)$. J. Alloys Compd. **507**, 405–409 (2010)
42. A. Selmi, R. M'nassri, W. Cheikhrouhou-Koubaa, N. Chniba Boudjada, A. Cheikhrouhou, Effects of partial Mn-substitution on magnetic and magnetocaloric properties in $Pr_{0.7}Ca_{0.3}Mn_{0.95}X_{0.05}O_3$ (Cr, Ni, Co and Fe) manganites. J. Alloys Compd. **619**, 627–633 (2015)
43. P. Nisha, S. Savitha Pillai, A. Darbandi, M.R. Varma, K.G. Sureshand Horst Hahn, Critical behaviour and magnetocaloric effect of nano crystalline $La_{0.67}Ca_{0.33}Mn_{1-x}Fe_xO_3$ (x = 0.05, 0.2) synthesized by nebulized spray pyrolysis. Mater. Chem. Phys. **136**, 66–74 (2012)
44. P. Zhang, H. Yang, S. Zhang, H. Ge, S. Hua, Magnetic and magnetocaloric properties of perovskite $La_{0.7}Sr_{0.3}Mn_{1-x}Co_xO_3$. Phys. B **410**, 1–4 (2013)
45. E. Oumezzine, S. Hcini, E.K. Hlil, E. Dhahri, M. Oumezzine, Effect of Ni-doping on structural, magnetic and magnetocaloric properties of $La_{0.6}Pr_{0.1}Ba_{0.3}Mn_{1-x}Ni_xO_3$ nanocrystalline manganites synthesized by Pechini sol-gel method. J. Alloys Compd. **615**, 553–560 (2014)
46. V.K. Pecharsky, K.A. Gschneidner, Magnetocaloric materials. Annu. Rev. Mater. Sci. **30**, 387–429 (2000)
47. B.K. Banerjee, On a generalised approach to first and second order magnetic transitions. Phys. Lett. **12**, 16–17 (1964)
48. A.O. Ayaş, Structural and magnetic properties with reversible magnetocaloric effect in $PrSr_{1-x}Pb_xMn_2O_6$ $(0.1 \leq x \leq 0.3)$ double perovskite manganite structures. Philos. Mag. **98**(30), 2782–2796 (2018)
49. C.M. Bonilla, J. Herrero-Albillos, F. Bartolome, L.M. Garcia, M. Parra-Borderias, V. Franco, Universal behavior for magnetic entropy change in magnetocaloric materials: an analysis on the nature of phase transitions. Phys. Rev. B **81**, (2010)
50. J.S. Amaral, M.S. Reis, V.S. Amaral, T.M. Mendonc¸a, J.P. Araújo, M.A. Sá, P.B. Tavares, J.M. Vieira, Magnetocaloric effect in Er- and Eu-substituted ferromagnetic La-Sr manganites. J. Magn. Magn. Mater. **290**, 686–689 (2005)
51. A. Krichene, W. Boujelben, Enhancement of the magnetocaloric effect in composites based on $La_{0.4}Re_{0.1}Ca_{0.5}MnO_3$ (Re= Dy, Gd, and Eu) polycrystalline manganites. J. Supercond. Novel Magn. **31**, 577–582 (2018)
52. J. Fan, L. Pi, L. Zhang, W. Tong, L. Ling, B. Hong, Y. Shi, W. Zhang, D. Lu, Y. Zhang, Magnetic and magnetocaloric

properties of perovskite manganite $Pr_{0.55}Sr_{0.45}MnO_3$. Phys. B **406**, 2289–2292 (2011)
53. R. Guetari, T. Bartoli, C.B. Cizmas, N. Mliki, L. Bessais, Structure, magnetic and magnetocaloric properties of new nanocrystalline (Pr, Dy)Fe_9 compounds. J. Alloys Compd. **684**, 291–298 (2016)
54. A. Fujita, K. Fukamichi, Large magnetocaloric effects and landau coefficients of itinerant electron metamagnetic La(Fe_xSi_{1-x})13 compounds. IEEE Trans. Magn. **41**, 3490–3492 (2005)
55. M. Koubaa, Y. Regaieg, W.C. Koubaa, A. Cheikhrouhou, S. Ammar-Merah, F. Herbst, Magnetic and magnetocaloric properties of lanthanum manganites with monovalent elements doping at A-site. J. Magn. Magn. Mater. **323**, 252–257 (2011)
56. R. Cherif, E.K. Hlil, M. Ellouze, F. Elhalouani, S. Obbade, Study of magnetic and magnetocaloric properties of $La_{0.6}Pr_{0.1}Ba_{0.3}MnO_3$ and $La_{0.6}Pr_{0.1}Ba_{0.3}Mn_{0.9}Fe_{0.1}O_3$ perovskite-type manganese oxides. J. Mater. Sci. **49**, 8244–8251 (2014)
57. H. Yang, P. Zhang, Q. Wu, H. Ge, M. Pan, Effect of monovalent metal substitution on the magnetocaloric effect of perovskite manganites $Pr_{0.5}Sr_{0.3}M_{0.2}MnO_3$ (M=Na, Li, K and Ag). J. Magn. Magn. Mater. **324**, 3727–3730 (2012)